J Electroceram (2009) 23:43–51
DOI 10.1007/s10832-008-9520-4

Preparation and electrical properties of Ni/(Ba,Sr)TiO_3 PTC composite with low resistivity

Xiaoyan Li · Yuanfang Qu · Jing Gao

Received: 2 January 2008 / Accepted: 25 April 2008 / Published online: 13 May 2008

Abstract Ni/ (Ba,Sr)TiO_3 PTC composite of low resistivity was fabricated by a solid state route. A mildly reducing sintering atmosphere was employed to avoid the oxidation of nickel. Metallic nickel is the main chemical state after sintering in the mildly reducing sintering atmosphere. With the increase in nickel amount, the room-temperature resistivity declines and the PTC effect worsens. The quantum mechanical tunneling effect at the Ni–(Ba,Sr)TiO_3 interface is presumably the prime factor in the deterioration of the PTC effect. PbO–B_2O_3–ZnO–SiO_2 glass was added to modify the interface between nickel and (Ba,Sr)TiO_3 ceramics. The intergranular phase introduced by the glass has an amorphous structure and exists at the interfaces and triple junctions of (Ba,Sr)TiO_3 grains and nickel grains. No obvious diffusion occurs at the interface between crystalline (Ba,Sr)TiO_3 grain and the intergranular phase. Also the added-glass improves the distribution of metal phase. The proper glass addition screens interfacial electron tunneling effect and improves the composite electrical properties. An abundance of the intergranular phase due to excess glass will, however, result in high room-temperature resistivity. The influences of nickel amount and glass amount on the microstructure evolution and electrical properties were analyzed.

X. Li (✉) · Y. Qu
Key Laboratory for Advanced Ceramics
and Machining Technology of Ministry of Education,
Tianjin University,
Tianjin 300072, China
e-mail: sophia145@gmail.com

J. Gao
AMI DODUCO (Tianjin) Electrical Contacts Manufacturing Co., Ltd,
Tianjin 300111, China

Keywords (Ba,Sr)TiO_3 · PTC (positive temperature coefficient) composite · Ni (nickel) · Electrical properties

1 Introduction

Donor-doped $BaTiO_3$ ceramics with a positive temperature coefficient resistance (PTCR) effect have been used extensively in electronic industry, such as over-current protectors, temperature sensors and self-regulating heaters [1]. However, challenges still exist in these applications, especially in microelectronic circuits working at low voltage, where the relatively high room-temperature resistivity of $BaTiO_3$-based PTC ceramics results in application restriction [2, 3]. From a Japanese patent, adding metal to $BaTiO_3$-based PTC ceramics to form composite has been one of the effective ways to reduce the room-temperature resistivity of semiconducting $BaTiO_3$ ceramics [4]. When metal is added to the ceramic matrix, the electrical property of the composite is determined by the co-functions of ceramic matrix and metal. The interfacial reaction should be investigated as much as possible so that the processing can be controlled and electrical properties can be optimized. However, in the reference [5], metal was just regarded as low-resistance phase. Though in the limited literature [1, 3, 6], metal–ceramics (M–C) contact was considered as Ohmic contact, the details of the M–C interface were not considered. Furthermore, there seemed to be no experimental work in the previous literature to improve such M–C interfaces in the metal/ceramics PTC composite.

In the present work, metal nickel has been chosen as the candidate. The Ohmic contact mechanism at M–C interfaces and its influence on the composite PTC effect are interpreted. On the other hand, PbO–B_2O_3–SiO_2 glass is always added into electrode paste of metals, which can be

used for PTCR semiconducting ceramics [7–10]. The glass provides good adhesion between the electrode metal and PTC ceramics and accordingly enhances the electrode–ceramics interfaces. Considering the facts above, an attempt has been made to use the similar glass composition to improve the interfaces between metal Ni and $BaTiO_3$-based PTC ceramics. The present study focuses on the changes (i.e. microstructural and electrical) that occur to the ceramic matrix and M–C interfaces.

In general, the metal/$BaTiO_3$ composite needed to be sintered in a reducing atmosphere to avoid the oxidation of metal [1, 3, 11]. However, such a reducing atmosphere resulted in a poor PTC effect or no PTC effect due to desorption of grain boundary oxygen [12]. In the present work, a mildly reducing atmosphere has been employed.

2 Experimental procedure

2.1 Glass preparation

The low melting glass was based on the $PbO{\cdot}B_2O_3{\cdot}ZnO{\cdot}SiO_2$ composition in the relative weight ratio of 71.5:12.5:15.0:1.0. Calculated amount of reagent–agent chemicals (Pb_3O_4, H_3BO_3, ZnO and SiO_2) were weighed, mixed, and melted in a covered crucible in air atmosphere at 820°C for 30 min. The molten glass was quenched on a platinum plate cooled by water. The glass was then crushed and sieved to pass through an 80 mesh screen. The softening point of glass was 380°C.

2.2 Samples fabrication

Table 1 shows the typical material composition throughout the present work. The PTC material was prepared by the conventional powder mixing procedure. The raw materials $BaCO_3$, $SrCO_3$, TiO_2, Sb_2O_3 and Nb_2O_5 were weighed according to the formula: $(Ba_{0.92}Sr_{0.08})TiO_3$ + 0.06 mol% Sb_2O_3 + 0.11 mol% Nb_2O_5. These powders were mixed with deionized water for 4 h, dried, calcined at 1050°C for 2 h. The resulting material was mixed with 0.04 mol% MnO_2, 0.1 wt%AST (the mixture of Al_2O_3–SiO_2–TiO_2 at molar ratio 4:9:3) and glass in an agate planetary ball mill for 6 h and dried. The amount of glass ranged from 0 to 4 wt%.

Table 1 Typical material composition.

Sample no.	Ni (wt%)	Glass (wt%)
1	0	0
2	6	0
3	15	0
4	21	0
5	30	0
6	15	0.5
7	15	1
8	15	4

In the present study, Ni particles were spherical and the particle size was in the range 74–165 μm. The amount of Ni ranged from 3 to 40 wt%. Ni/$(Ba,Sr)TiO_3$ PTC composite was prepared by adding Ni powder to dried $(Ba,Sr)TiO_3$ matrix obtained above. The following mixing was performed using a mortar and pestle for 1 h. After granulation by passing through a 40 mesh powder sieve, the powders obtained were pressed into disk-shaped samples (10 mm diameter and 2 mm thickness) under a pressure of 300 MPa. The samples were sintered in a mildly reducing atmosphere produced by graphite powder (Samples were put on an Al_2O_3 setter in a bottom–up alumina crucible. Sufficient graphite powder was placed beside the samples in the crucible and there was no contact between the graphite powder and the samples). After sintering, the furnace was switched off and the samples were cooled down.

2.3 Microstructural analysis

X-ray diffraction (XRD, Rigaku D/max 2500v/pc) with Cu $K\alpha$ radiation was utilized to identify the phases of the sintered samples. X-ray photoelectron spectroscopy (XPS, PHI-5300, ESCA System) with an Mg Ka X-ray source (1253.6 eV) was used to analyze the surface electronic states. All XPS peaks were referenced to the C1s signal at a binding energy of 284.6 eV. A metallographic microscope (Leitz MM6 PL 2X-160X) was used to observe the polished surfaces of the samples. An environmental scanning electron microscope (ESEM, Philips XL-30) was employed in the observation of the sample morphology. Samples for TEM observation were mechanically thinned and Ar^+ -ion-beam milled after they have been mounted onto 3-mm Cu grid. A field emission gun TEM (Tecnai G^2 F-20) fitted with an energy-dispersive X-ray (EDX) spectrometer was used to analyze the interfacial microstructure and composition of the samples.

2.4 Electrical properties

After sintering, the samples were cleaned using an ultrasonic bath and electroded using Ag electrode slurry. The Ag electrode was dried under the light and treated at 490°C for 10 min. The variation of electrical resistivity with temperature was measured in a programmable muffle oven during heating (heating rate 3°C/min), using a digital multi-meter (Hewlett-Packard, 3457 A, the applied voltage is about 1 V).

3 Results and discussion

3.1 The effect of Ni addition and sintering atmosphere

3.1.1 Microstructure evolution

The microstructures of samples 1, 2 and 3 are displayed in Fig. 1. The microstructures are found to be inhomogeneous after the mixing of Ni powder, as seen in Fig. 1(b) and (c). Microstructural development in donor-doped $BaTiO_3$ is mainly determined by abnormal grain growth. This process is terminated when these rapidly growing grains impinge on each other [13]. In the composite, Ni particles locate at the ceramic grain boundaries and confine the abnormal grain growth of ceramics. The presence of metal coalescence or big metal particles causes severe deterioration of the microstructure.

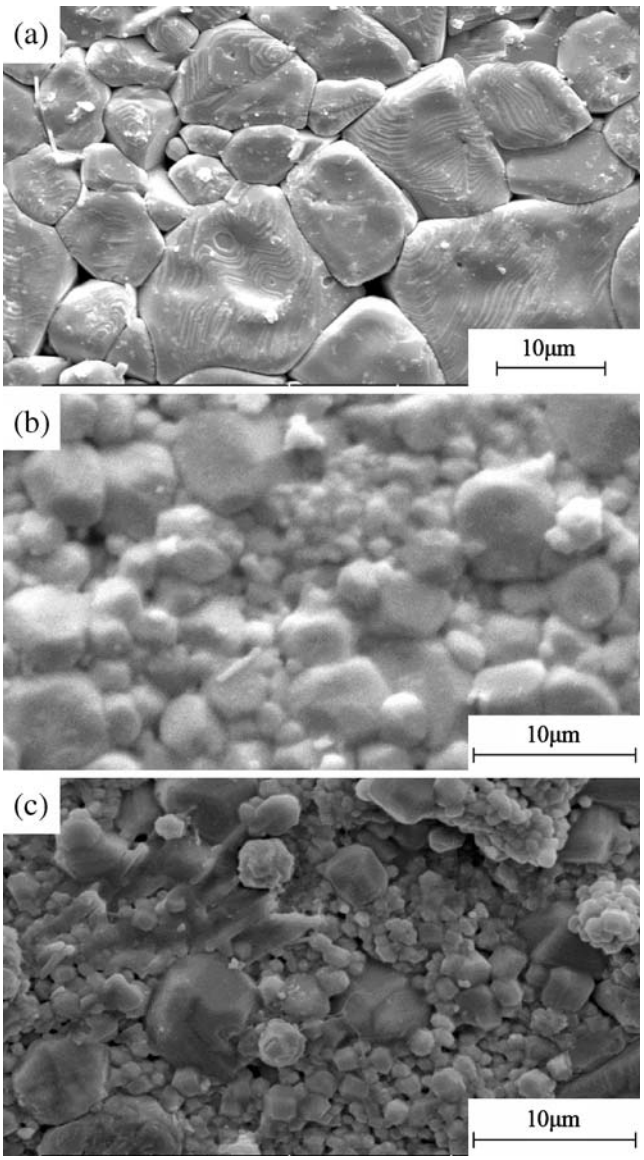

Fig. 1 SEM images of (**a**) sample 1, (**b**) sample 2 and (**c**) sample 3 (sintered at 1230°C for 20 min in the mildly reducing atmosphere)

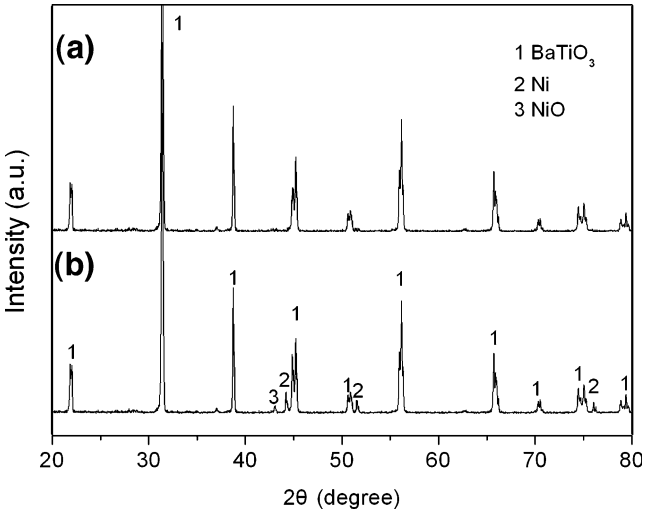

Fig. 2 X-ray diffraction patterns of (**a**) sample1 and (**b**) sample 3

3.1.2 Phase identification

The XRD patterns for sample 1 and 3 are shown in Fig. 2. Comparison with standard XRD files shows that peak splitting corresponding to tetragonal $BaTiO_3$ is evident in sample 1. Due to the low solid solution content of $SrTiO_3$, the diffraction peaks of sample 1 do not shift to high angle. XRD peaks of sample 3 indicate strong diffraction peaks of Ni and a faint diffraction peak of NiO. The mildly reducing atmosphere is practicable in preventing nickel particles from oxidation.

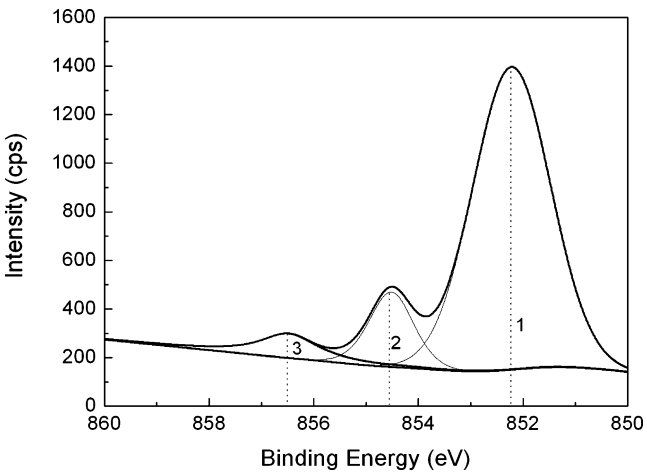

Fig. 3 XPS spectrum and fitted spectrum of nickel on the surface of sample 3

3.1.3 The chemical states of nickel

Figure 3 shows an XPS spectrum and its fitting spectrum of nickel on the surface of sample 3. The 2p3/2 peak 1 at 852.2 eV is characteristic of Ni (0). The 2p3/2 peaks 2 and 3, at 854.6 eV and 856.6eV respectively, are assigned as characteristic of Ni^{2+} in the NiO [14]. Due to the high peak intensity of Ni (0), the XPS analysis indicates that metallic nickel is the main chemical state after sintering in the mildly reducing atmosphere.

3.1.4 Ni–(Ba,Sr)TiO_3 interfaces

There are three types of Ni particles in the composite, namely, *a, b* and *c*, as shown in Fig. 4. If Ni particles locate at *a* or *c* sites, charge transport behavior at Ni–(Ba,Sr)TiO_3 interfaces is important. Due to the large number of surface states at the metal-semiconductor interface, selecting a metal with the right work function might still not result in the expected Ohmic contact. An alternate and more practical low-resistance contact is a tunnel contact. Such contacts do have a positive barrier at the metal-semiconductor interface, but also have a high enough doping in the semiconductor that there is only a thin barrier separating the metal from the semiconductor. If the width of the depletion region at the metal-semiconductor interface is very thin, on the order of 3 nm or less, carriers can readily tunnel across such barrier. The required doping density for such a contact is 10^{19} cm^{-3} or higher [15]. Based on the designed composition, the added donor concentration of (Ba,Sr)TiO_3 ceramics is estimated to be 5×10^{19} cm^{-3}. Considering the quantum mechanical tunneling effect, Ohmic contacts can be achieved. At the interface, shown in Fig. 5, electrons tunnel across the barrier between a nickel grain and a (Ba,Sr)TiO_3 grain, resulting in big tunneling current and negligible contact resistance. The presence of Ni–(Ba,Sr)TiO_3 interfaces leads to low room-temperature resistivity and weak PTC effect. On the other hand, when Ni particles locate at *b* sites, it is equivalent to decrease the thickness of the resistive grain boundary and thus lower the grain-boundary resistivity. In this case, there is no charge transfer between nickel and (Ba Sr)TiO_3 grains. Surface states and corresponding PTC effect are not greatly influenced. Generally speaking, surface states at the ceramic grain boundaries and corresponding electrical potential barriers are responsible for the PTC effect in the composite.

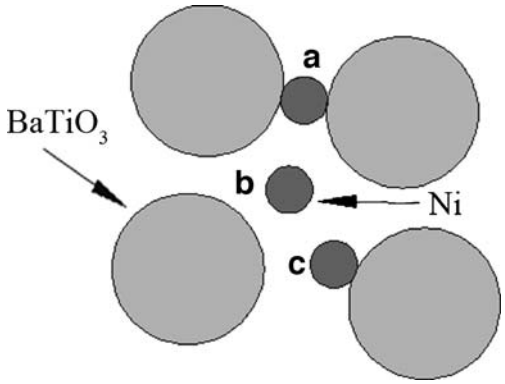

Fig. 4 Schematic figure of Ni/$BaTiO_3$ composite

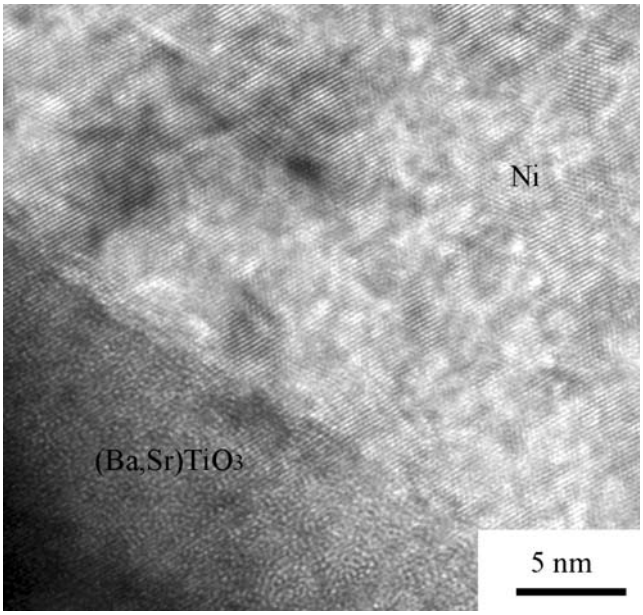

Fig. 5 HRTEM micrograph of the interface between the nickel grain and the (Ba,Sr)TiO_3 grain in sample 3

3.1.5 PTC effect

Figure 6 shows the resistivity-temperature characteristics of (Ba,Sr)TiO_3 ceramics and Ni/(Ba,Sr)TiO_3 composite. The

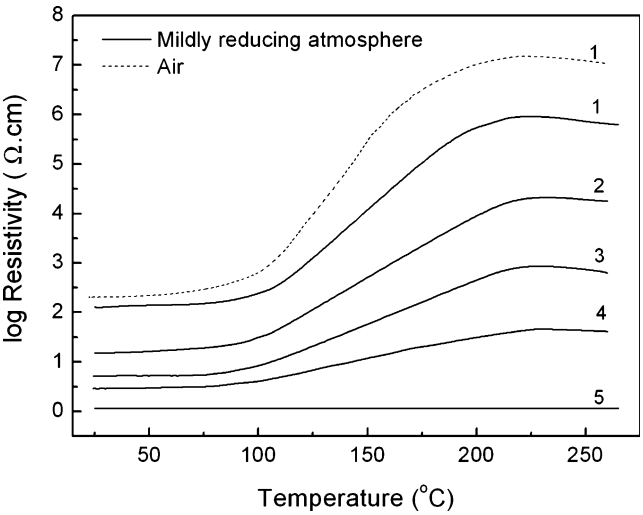

Fig. 6 Temperature dependence of resistivity of (Ba,Sr)TiO_3 ceramics and composites with different nickel amounts [*broken line* for (Ba,Sr)TiO_3 ceramics sintered in air and *straight line* for samples sintered in the mildly reducing atmosphere]

sintering is kept at 1230°C for 20 min. The room-temperature resistivity of $(Ba,Sr)TiO_3$ ceramics sintered in air and in the mildly reducing atmosphere equals 162 and 127 Ω cm, respectively. After 6 wt% Ni powder is added, room-temperature resistivity of composite sharply decreases to 15 Ω cm. However, further increase in Ni amount decreases the room-temperature resistivity moderately. All curves in Fig. 6 show nearly the same temperature at which the dramatic increase in resistivity begins. It can be seen that the mildly reducing atmosphere slightly reduces the PTC jump of $(Ba,Sr)TiO_3$ ceramics, about one order of magnitude. PTC effect deteriorates with the increasing Ni amount and when the Ni amount exceeds 30 wt%, there is no PTC effect observed.

PTC effect of $(Ba,Sr)TiO_3$ ceramics can be explained by the traditional PTC models. Above the Curie temperature (Tc), a potential barrier develops between the bulk and the insulating grain-boundary region. The barrier results in a high resistivity for charge transfer across the grain boundary. Below Tc the barrier is significantly decreases as a result of the charge compensation effect produced by electrical polarization [16]. Weaker PTC effect after sintering in the mildly reducing atmosphere can be attributed to the low oxygen partial pressure [16, 17].

After the introduction of Ni powder, the restrained grain growth leads to a large amount of small ceramic grains. The thickness of the insulting layer becomes comparable to the size of the semiconducting grains. Moreover, the spontaneous polarization due to the phase transition is too small to compensate for the electron traps. The lowering in potential barrier height below Tc is limited. A large room-temperature resistivity and poor PTC effect thus result in the ceramic matrix. Besides the electrical properties of the constituent ceramics and nickel phases, charge transport behavior at Ni–$(Ba,Sr)TiO_3$ interfaces should be considered. Above Tc, the potential barrier at Ni–$(Ba,Sr)TiO_3$ interfaces is completely negligible due to the Ohmic contact. The higher the Ni amount, the more Ni–$(Ba,Sr)TiO_3$ interfaces and the worse the PTC effect. When the Ni amount reaches 30 wt%, few ceramic grain boundaries exist. Electrons flow only through the nickel grains, semiconducting ceramic grains and Ni–$(Ba,Sr)TiO_3$ interfaces, which is believed to cause the absence of PTC effect in the composite.

3.2 The effect of glass

3.2.1 Phase distribution

Metallographic microscope images of polished surfaces of sample 3 and 6 are displayed in Fig. 7. Three different phases are obviously observed. The bright disperse phase is nickel. The dark continuous phase is ceramic matrix and the even darker phase is found to be the grain-boundary phase and the pores. Added-glass produces a microstructural effect, bringing out a reduction in nickel particle size and more homogeneous distribution of nickel particles.

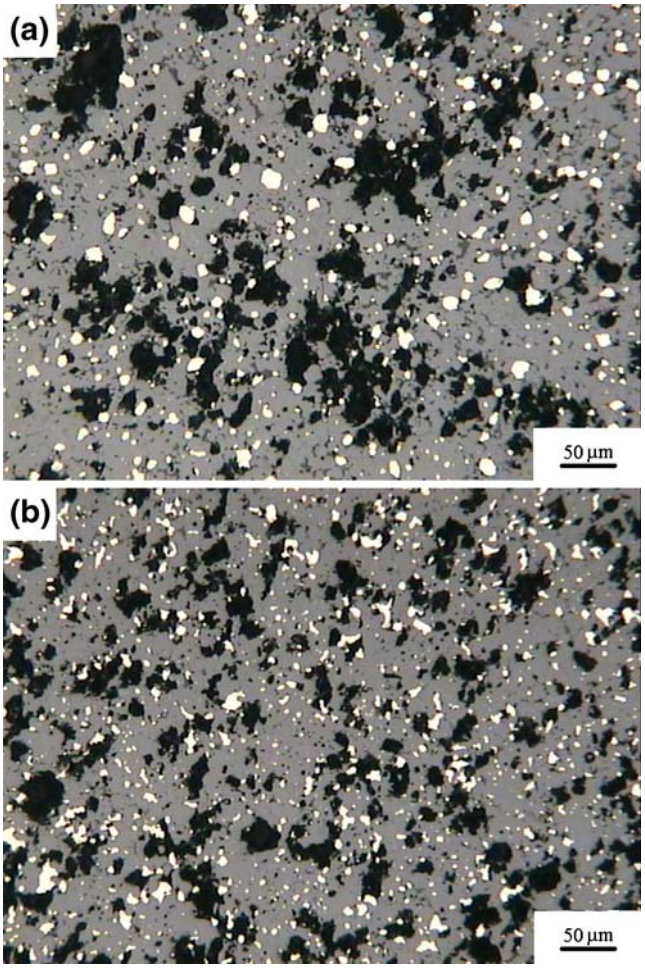

Fig. 7 Metallographic microscope images of polished surface of (**a**) sample 3 and (**b**) sample 6 (Sintered at 1320°C for 20 min)

SEM images of sample 3 and 6 and corresponding elemental mappings of nickel are displayed in Fig. 8. Compared with the image in Fig. 1(c), the microstructure of sample 3 is modified remarkably after sintering at 1320°C. The tiny ceramic grains (<2 μm) in Fig. 1(c) are almost eliminated. In other words, the driving force for grain growth increases with the increasing sintering temperature, thus the grain growth inhibition due to the nickel addition is weakened. The addition of glass leads to bigger ceramic grains and narrow-size distribution in sample 6. It is interesting to observe from Fig. 8(c) and (d) that Ni particles in sample 6 are more homogeneously distributed in the ceramic matrix than those in sample 3. This is consistent with the observation on the metallographic microscope. This can probably be ascribed to the low viscosity and better fluidity of the glass with high PbO

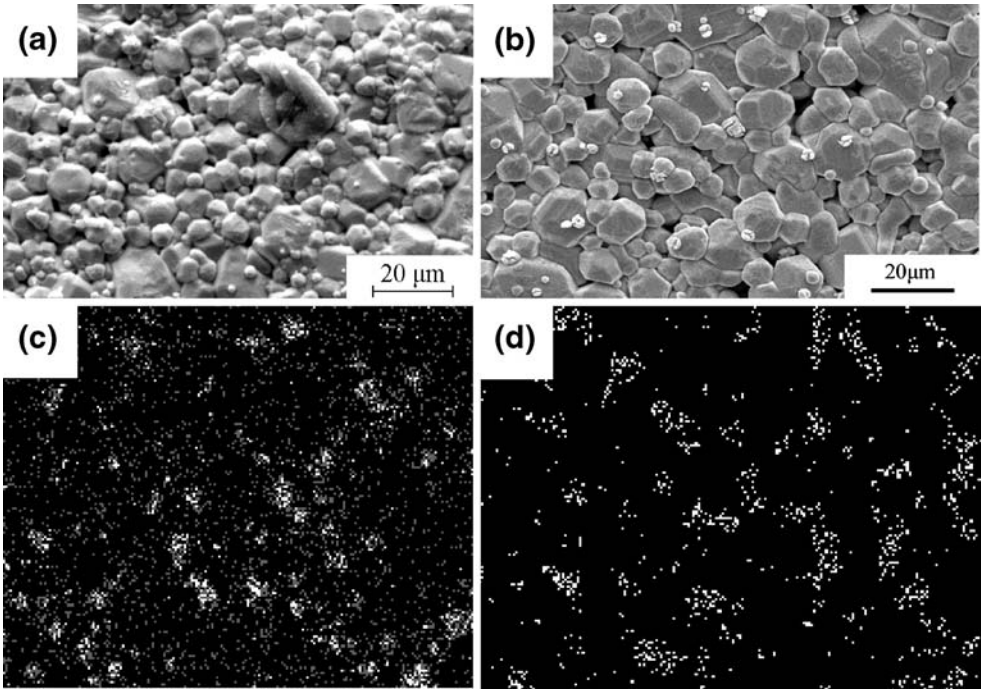

Fig. 8 SEM images of (**a**) sample 3, (**b**) sample 6 and corresponding elemental mapping of nickel in (**c**) sample 3, (**d**) sample 6 (Sintered at 1320° C for 20 min)

content, which enhances the particle rearrangement process of ceramic and metal grains [18].

3.2.2 Phase interfaces

Figure 9 shows the TEM image of an intergranular phase between grains in sample 8. The width of the intergranular region varies greatly from a few nanometers to 200 nm. Also solidified liquid phase locates at triple junctions. It is worth mentioning that, the adjacent grains might be (Ba,Sr)TiO_3 or nickel grains.

TEM-electron diffraction and TEM-EDX were used to provide more detailed information of the composite. Figure 10 shows the TEM micrograph and selected area electron diffraction pattern of sample 8. The selected area diffraction (SAD) pattern labeled (a) taken from the grain on the left side indicates that it is a crystalline grain of (Ba,Sr)TiO_3 in [010] crystal axis. The SAD pattern labeled (b) taken from the grain on the right side indicates that it is a nickel grain in [$\bar{1}$11] crystal axis. The SAD pattern labeled (c) taken from the intergranular phase shows that it has an amorphous structure.

The high resolution TEM image in Fig. 11 shows the interface between a crystalline (Ba,Sr)TiO_3 grain and the intergranular phase. No obvious diffusion between them can be observed. EDX measurements were carried out at positions along a line that traverses the (Ba,Sr)TiO_3 grain, intergranular phase and nickel grain. The line position is shown in Fig. 10. As seen in Fig. 12, Pb, Ba and Ti were detected in the intergranular phase, but no other glass components such as B, Si, Zn were detectable.

3.2.3 PTC effect

The resistivity-temperature characteristics of composites with different amounts of glass are shown in Fig. 13. 0.5 wt% glass-added sample 6 shows an enhanced PTC effect. The magnitude of PTC jump is one order of magnitude higher than that of glass-free sample 3. It is interesting to note that the room-temperature resistivity is sharply increased and the PTC jump is slightly decreased with further increase in the glass amount.

With low glass amount, capillarity shortens the gaps between Ni and (Ba,Sr)TiO_3 grains and thus enhances the tunneling current. However superabundant glass leads to the gaps between Ni and (Ba,Sr)TiO_3 grains too large to

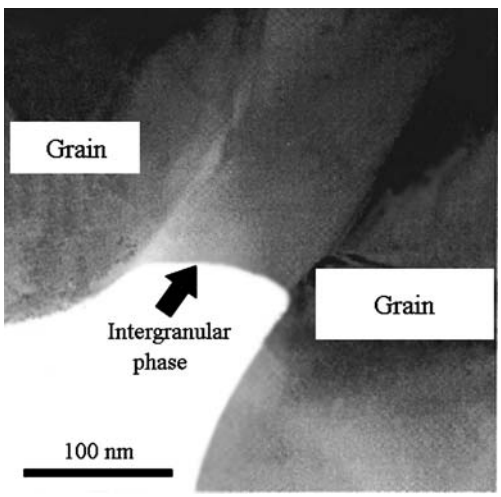

Fig. 9 TEM micrograph of the intergranular phase in sample 8

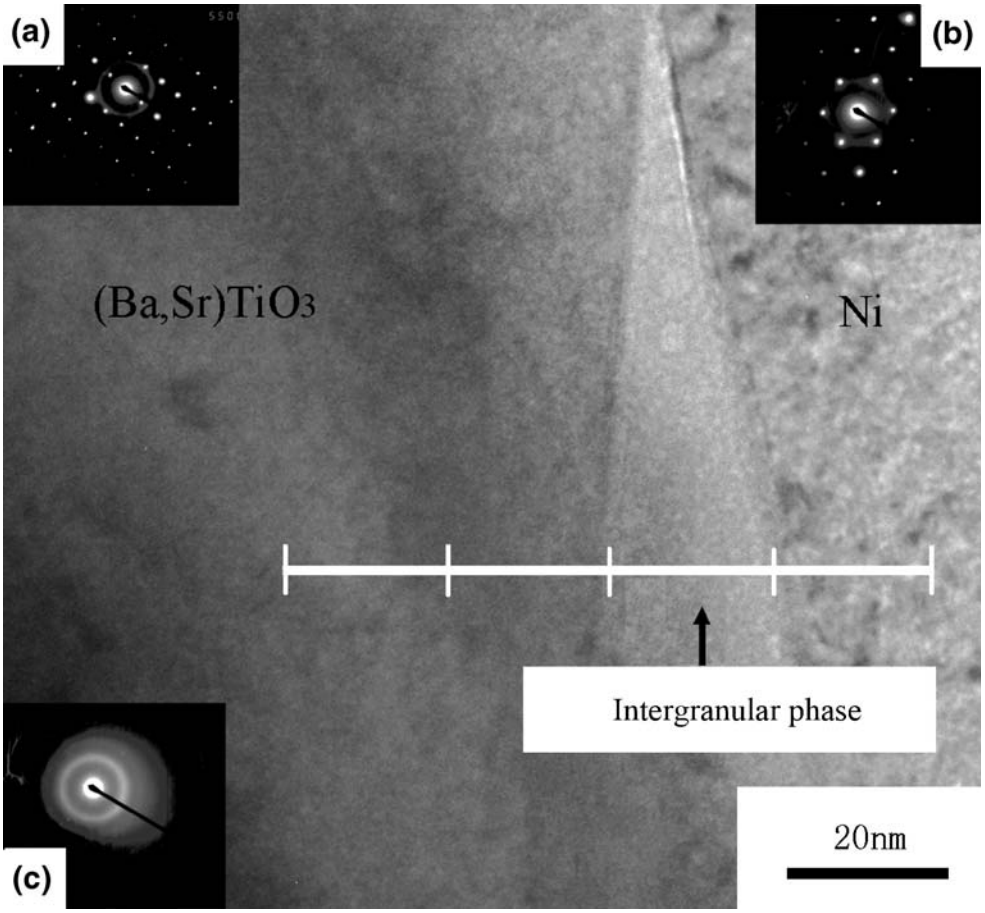

Fig. 10 TEM micrograph and selected area electron diffraction pattern of the (**a**) grain on the left side, (**b**) grain on the right side and (**c**) intergranular phase of sample 8

allow electron tunneling. The excessive glass leads to the increase in thickness of the intergranular phase and the break-up of conducting chains, similar to the break-up of conducting chains after thermal volume expansion in carbon black loaded polymer PTC composite, discussed by Ohe and Nitio [19]. In the glass-excess case, no charge transfer occurs between ceramic and nickel grains. The glass with enveloped nickel particles serves as the ceramic grain-boundary phase. The nickel particle in this case finds its equivalent in *b* site, shown in Fig. 4. The grain-boundary

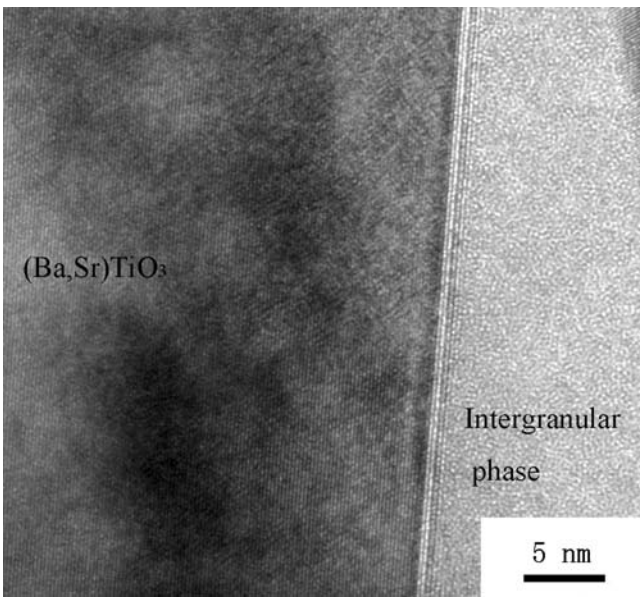

Fig. 11 HRTEM micrograph of the interface between the $(Ba,Sr)TiO_3$ grain and the intergranular phase in sample 8

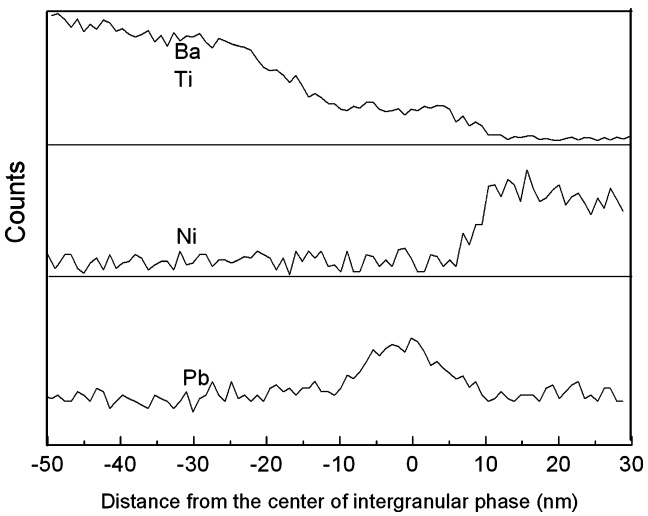

Fig. 12 EDX intensity along the line across the $(Ba,Sr)TiO_3$ grain, intergranular phase and nickel grain

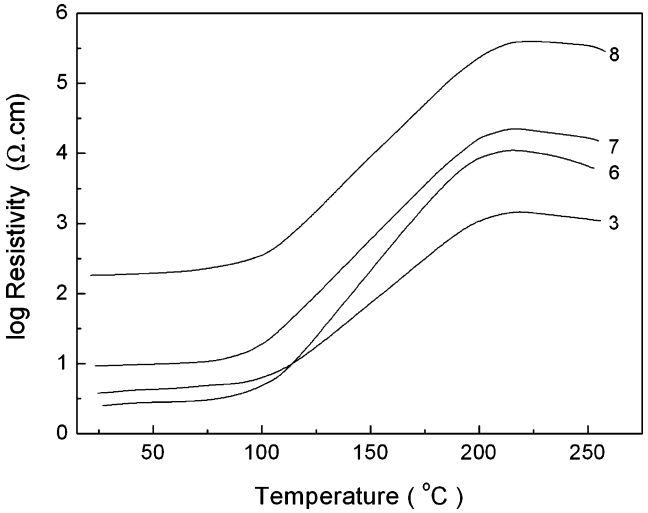

Fig. 13 Temperature dependence of resistivity of composites with different glass amounts

resistance is determined by the relative amount of high-resistance glass and low-resistance nickel. With the high amount of glass in sample 8, the effect of nickel in decreasing the grain-boundary resistance can be neglected. The high grain-boundary resistance leads to high room-temperature resistivity and low PTC jump.

The composite PTC effect is also closely related to the phase distribution. When the system contains a non-homogeneous nickel distribution, in the nickel enriched regions, conducting electrons primarily flow through semiconducting ceramic grains, nickel grains and Ni–(Ba,Sr)TiO_3 interfaces. The potential barrier is low due to tunneling effect. Conversely, in the nickel deficient regions, no local electrons flow through ceramic grain-boundaries as the conducting electrons always follow the path with the lowest barrier, which exists in the nickel enriched regions. The presence of metal coalescence or big metal particles leads to poor PTC effect in glass-free sample 3. As the glass addition improves the distribution of nickel particles, there is no short-cut path for conducting electrons. Surface states related to the ceramic grain-boundaries are activated, required for the formation of electron traps and resulting potential barrier, which is in contrast to the inactive surface states in sample 3.

For the particular system studied, lower room-temperature resistivity and considerable PTC effect are acquired in sample 6. It is ascribed to the homogeneous distribution of nickel particles and the proper intergranular layer, which effectively avoids electron tunneling and PTC deterioration. Also the intergranular layer is thin enough not to greatly increase grain-boundary resistance.

Figure 14 shows the PTC behavior for sample 6, exposed to three thermal cycles. It is clearly seen that there is a tendency of increase in the room-temperature resistivity after three measurements. The maximum resistivity remains almost unchanged. The room-temperature resistivity at the first measuring is 2.5 Ω cm, while the room-temperature resistivity becomes 3.5 Ω cm at the second measuring. After that, the room-temperature resistivity increase is negligible.

4 Conclusions

(1) When a Ni/(Ba,Sr)TiO_3 composite is sintered under the mildly reducing atmosphere, nickel metal is the main chemical state of introduced metal phase. Although there exists a small quantity of NiO, a composite with low resistivity is obtained. The mildly reducing atmosphere with low oxygen partial pressure reduces the magnitude of the PTC effect in (Ba,Sr)TiO_3 ceramics by one order of magnitude.

(2) Grain growth of ceramics is restrained after the introduction of nickel powder. Severe deterioration of the microstructure due to nickel addition is weakened by high sintering temperature and the addition of PbO–B_2O_3–ZnO–SiO_2 glass.

(3) The introduction of nickel to (Ba,Sr)TiO_3 ceramic matrix markedly reduces the room-temperature resistivity. The Ohmic contact at Ni–(Ba,Sr)TiO_3 interfaces leads to a weak PTC effect and should be avoided. Nickel particles are preferred to locate at the ceramic grain boundaries and not to exchange charge with ceramic grains in the system studied.

(4) PbO–B_2O_3–ZnO–SiO_2 glass added to the Ni/(Ba,Sr)TiO_3 composite not only improves the rearrangement of nickel and ceramic grains but also modifies the metal-ceramics interfaces. The quantum mechanical tunneling effect can be neglected when the gap between nickel and ceramic grains due to the glass

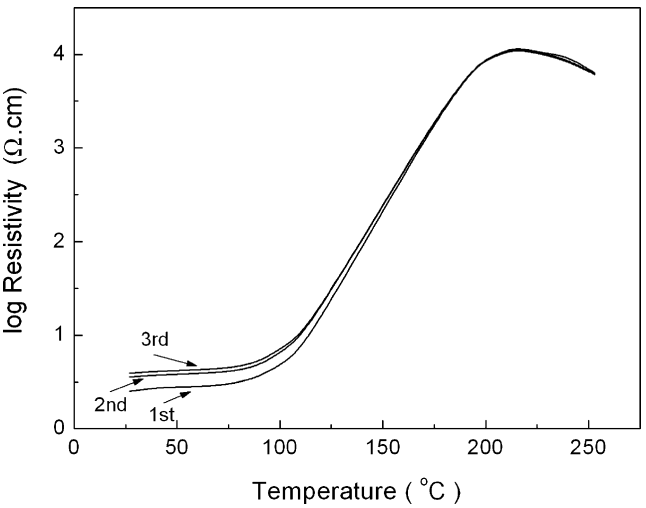

Fig. 14 Resistivity-temperature characteristics of sample 6, exposed to three thermal cycles

addition is large enough. For a composite possessing low room-temperature resistivity and considerable PTC effect, an intergranular layer with a suitable thickness is desirable.

Acknowledgement The authors would like to acknowledge the support of Key Laboratory for Advanced Ceramics and Machining Technology of Ministry of Education.

References

1. J. Du, Y.F. Qu, W.B. Ma, J. Electro-ceram. **12**(3), 163 (2004). DOI 10.1023/B:JECR.0000037721.69456.a1
2. Z.Z. Huang, S.U. Adikary, H.L.W. Chan, C.L. Choy, J. Mater. Sci. Mater. Electron. **13**, 221 (2002). DOI 10.1023/A:1014879917445
3. Z.M. He, J. Ma, Y.F. Qu, C.G. Wang, J. Eur. Ceram. Soc. **24**, 3617 (2004). DOI 10.1016/j.jeurceramsoc.2003.12.015
4. I. Yoshiyuki, K. Naoki, Japanese Patent, JP 58 028 803 (1983)
5. Z.M. He, J. Ma, Y.F. Qu, X.M. Feng, J. Eur. Ceram. Soc. **22**, 2143 (2002). DOI 10.1016/S0955-2219(01)00538-6
6. Z.M. He, J. Ma, J. Mater. Sci. Mater. Electron. **11**, 235 (2000). DOI 10.1023/A:1008901000485
7. C.Y. Deng, X.F. Li, L.L. Xiao, S.L. Jiang, Y.K. Zeng, J. Func. Mater. **36**(5), 692 (2005) (in Chinese)
8. W.T. Sun, Elecron. Compon. Mater. **16**(3), 14 (1997) (in Chinese)
9. Y. Chen, L. Guo et al., Piezoelectrics and Acoustooptics. **27**(1), 85 (2005) (in Chinese)
10. X.M. He, S.L. Liu et al., J. Func. Mater. **27**(5), 407 (1996) (in Chinese)
11. T. Kanou, T. Sawaguchi et al., J. Jpn. Soc. Power, Power Metall. **46**(7), 752 (1999)
12. I.C. Ho, S.L. Fu, J. Am. Ceram. Soc. **75**(3), 728 (1992). DOI 10.1111/j.1151-2916.1992.tb07869.x
13. I. Zajc, M. Drofenik, Br. Ceram. Trans. **88**, 223 (1989)
14. C.D. Wagner, W.M. Riggs, L.E. Davis et al., *Handbook of X-ray Photoelectron Spectroscopy* (Perkin-Elmer Corporation, Minnesota, 1979)
15. B.V. Zeghbroeck, Principles of semiconductor devices, Web-based book, University of Colorado at Boulder, 2004. URL: http://ece-www.colorado.edu/bart/book
16. J. Nowotny, M. Rekas, Ceram. Int. **17**, 227 (1991). DOI 10.1016/0272-8842(91)90017-T
17. T. Kolodiazhnyi, A. Petric, J. Am. Ceram. Soc. **86**(9), 1554 (2003)
18. S.F. Wang, T.C.K. Yang, Y.R. Wang, Y. Kuromitsu, Ceram. Int. **27**, 157 (2001). DOI 10.1016/S0272-8842(00)00055-9
19. K. Ohe, Y. Nitio, Jpn. J. Appl. Phys. **10**(1), 99 (1971). DOI 10.1143/JJAP.10.99